

Proton-implanted CeO_2/Sb_2O_3-co-doped phosphate glass waveguides and its annealing evolution

Chun-Xiao Liu(刘春晓), Shi-Yu Chen(陈诗语), Jia-Pei Wu(吴佳佩), Quan-Long He(贺全龙), Jian-Fei Guan(关建飞), Liao-Lin Zhang(张料林), and Hai-Tao Guo(郭海涛)

Citation: Chin. Phys. B, 2026, 35 (**8**): 084207. DOI: 10.1088/1674-1056/ae156d
http://cpb.iphy.ac.cn; http://iopscience.iop.org/cpb

What follows is a list of articles you may be interested in

Guiding and magneto-optical properties of TGG waveguide by proton implantation combined with femtosecond laser ablation

Chun-Xiao Liu(刘春晓), Zi-Hao Wang(王子昊), Bei-Er Guo(郭贝尔), Rui Yuan(袁睿), Yi-Fan Wang(王逸凡), Yu-Hang Zhou(周雨航), Jia-Bin Sun(孙家彬), Liao-Lin Zhang(张料林), and Hai-Tao Guo(郭海涛)
Chin. Phys. B, 2025, 34 (**5**): 054207. DOI: 10.1088/1674-1056/adb9cc

Experimental demonstration of silicon nitride waveguide gratings with excellent efficiency and divergence angle

Zhaozhen Chen(陈兆震), Wenling Li(李文玲), Qian Wang(王乾), Enfeng Liu(刘恩峰), Xinqun Zhang(张新群), Jingwei Liu(刘敬伟), and Zhengsheng Han(韩郑生)
Chin. Phys. B, 2025, 34 (**5**): 054206. DOI: 10.1088/1674-1056/adbbbf

Frequency-tunable single-photon router based on a microresonator containing a driven three-level emitter

Jin-Song Huang(黄劲松), Jing-Lan Hu(胡菁兰), Yan-Ling Li(李艳玲), and Zhong-Hui Xu(徐中辉)
Chin. Phys. B, 2024, 33 (**6**): 064202. DOI: 10.1088/1674-1056/ad362a

Singular optical propagation properties of two types of one-dimensional anti-*PT*-symmetric periodic ring optical waveguide networks

Yanglong Fan(樊阳龙), Xiangbo Yang(杨湘波), Huada Lian(练华达), Runkai Chen(陈润楷),Pengbo Zhu(朱蓬勃), Dongmei Deng(邓冬梅), Hongzhan Liu(刘宏展), and Zhongchao Wei(韦中超)
Chin. Phys. B, 2024, 33 (**3**): 034201. DOI: 10.1088/1674-1056/ad12ab

Bidirectional highly-efficient quantum routing in a T-bulge-shaped waveguide

Jia-Hao Zhang(张家豪), Da-Yong He(何大永), Gang-Yin Luo(罗刚银), Bi-Dou Wang(王弼陡), and Jin-Song Huang(黄劲松)
Chin. Phys. B, 2021, 30 (**3**): 034204. DOI: 10.1088/1674-1056/abd38c

---

Proton-implanted CeO_2/Sb_2O_3-co-doped phosphate glass waveguides and its annealing evolution

Chun-Xiao Liu(刘春晓)[1,†], Shi-Yu Chen(陈诗语)[1], Jia-Pei Wu(吴佳佩)[1], Quan-Long He(贺全龙)[2], Jian-Fei Guan(关建飞)[1], Liao-Lin Zhang(张料林)[3], and Hai-Tao Guo(郭海涛)[4]

[1] *College of Electronic and Optical Engineering, Nanjing University of Post and Telecommunications, Nanjing* 210023, *China*
[2] *Logging Technology Research Institute, China National Logging Corporation, Xi'an* 710077, *China*
[3] *School of Material Science and Engineering, Jiangxi University of Science and Technology, Ganzhou* 341000, *China*
[4] *State Key Laboratory of Transient Optics and Photonics, Xi'an Institute of Optics and Precision Mechanics, Chinese Academy of Sciences (CAS), Xi'an* 710119, *China*

(Received 15 September 2025; revised manuscript received 20 October 2025; accepted manuscript online 21 October 2025)

Proton implantation has received increasing attention in the field of optical waveguide fabrication. It is meaningful to explore the annealing effects on the guiding properties of the proton-implanted waveguides. In this work, the CeO_2/Sb_2O_3-co-doped phosphate glass waveguides were formed by 400-keV proton implantation, and the proton fluence was chosen to be 8×10^{16} ions/cm^2. The implanted glass was annealed in a series of 60-min thermal treatments at temperatures ranging from 260 °C to 360 °C. After each annealing treatment, the modes and their effective refractive indices were measured at 632.8 nm by a prism coupling system. The near-field intensity distribution of the zeroth-order mode was recorded by using an end-face coupling method. The mechanism of the planar waveguide formation is discussed by simulating the energy loss distribution and calculating the refractive index profile. It can enhance theoretical and experimental references for the development of integrated photonic devices by implantation and annealing.

Keywords: optical waveguide, proton implantation, CeO_2/Sb_2O_3-co-doped phosphate glass, thermal treatment

PACS: 42.79.Gn, 61.80.Jh

DOI: 10.1088/1674-1056/ae156d **CSTR:** 32038.14.CPB.ae156d

1. Introduction

In the fields of optical communications and integrated optics, optical waveguides play a dual core role: they are not only precision channels for directional transmission of optical signals, but also key bridges for efficient interconnection between optical devices.[1,2] Through an appropriate design of refractive index distribution, optical waveguides can effectively confine light waves within specific regions, achieving low propagation loss and precise coupling.[3,4] Hence, they provide reliable guarantees for the stable propagation of optical signals.[5,6] Thanks to the significant advantages of controllable production costs and highly integrated physical structures, optical waveguides are widely used in the research and development of various optical devices, becoming the fundamental components for building modern optical communication systems and micro optical chips.[7,8] From broadband networks to highly integrated photonic chips, optical waveguides with their outstanding performances are driving the continuous development of optoelectronic technology towards higher efficiency and smaller sizes.[9,10]

Due to the unique structure and important applications, the preparation and study of optical waveguides have received widespread attention from researchers.[11] Ion implantation is a material modification and doping technique, which was firstly used in metal surface modification and semiconductor doping.[12] Meanwhile, it is also a reliable method for the waveguide preparation.[13,14] By precisely controlling parameters such as energy, dose, and species during the ion implantation, key parameters including refractive index distribution and thickness of the optical waveguide can be accurately adjusted, thereby achieving precise control of the optical performance of the optical waveguide and meeting various requirements of different application scenarios.[15,16]

The novel material with unique optical and physical properties would expand the application fields of waveguides.[17] CeO_2/Sb_2O_3-co-doped phosphate glass is an indispensable raw material for many high-tech products in space-born star camera systems, because it has numerous technical characteristics including radiation resistance and material uniformity.[18] In addition, the CeO_2/Sb_2O_3-co-doped phosphate glass not only has excellent transparency, but also mechanical and chemical toughness. It would meet the technological optical requirements of integrated photonic devices for optical waveguides.

Although ion implantation can prepare waveguide structures, it inevitably causes damage and defects in the implanted

[†]Corresponding author. E-mail: chunxiaoliu@njupt.edu.cn

© 2026 Chinese Physical Society and IOP Publishing Ltd. All rights, including for text and data mining, AI training, and similar technologies, are reserved.

layer.[19] To repair these damage and defects to the maximum extent, it is necessary to perform thermal treatment on the ion-implanted sample at an appropriate time and temperature (this is called "annealing").[20] Moreover, the temperature and time of annealing treatment can affect the performance of ion-implanted waveguides.[21,22] To better understand the effect of annealing on waveguides, the proton implantation method followed by continuous thermal treatments is chosen to prepare waveguides in the CeO_2/Sb_2O_3-co-doped phosphate glass. This work takes the CeO_2/Sb_2O_3-co-doped phosphate glass waveguide and its evolution induced by the annealing as the research object, focusing on three key aspects: waveguide preparation, thermal treatment, and property comparison. To our knowledge, it is the first report that fabricates and optimizes the optical waveguide on the CeO_2/Sb_2O_3-co-doped phosphate glass. Moreover, a series of systematic and detailed works have been carried out, hoping to enhance theoretical and technical supports for the development of the CeO_2/Sb_2O_3-co-doped phosphate glass waveguide in space exploring and communications.

2. Experiments

For a given energy, the penetration range of protons is deepest among all ion implantations. Figure 1 shows the distributions of the projected range and longitudinal straggling in the energy range of 250 keV–550 keV for the H^+ ion implantation into the CeO_2/Sb_2O_3-co-doped phosphate glass. The projected range is 3.95 μm at the energy of 400 keV, which is the desired thickness for waveguide applications. Therefore, according to the results in Fig. 1, the CeO_2/Sb_2O_3-co-doped phosphate glasses were subjected to the H^+-ion implantation at 400-keV acceleration, 1.0-mA current, at room temperature. The fluence of the H^+ ions was 8×10^{16} ions/cm^2. The ion implantation was carried out by the 2×1.7-MV tandem accelerator of Peking University.

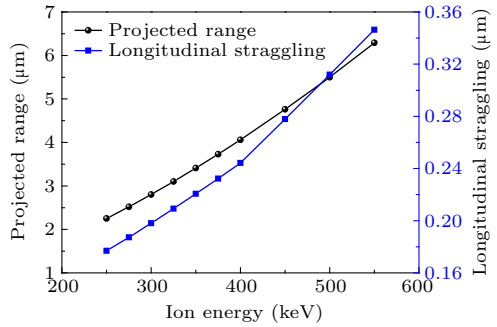


Fig. 1. Projected range and longitudinal straggling *versus* the ion energy.

The three-step annealing at intervals of 50 °C is used to study the effect of thermal treatment on waveguides. Table 1 lists the parameters for each annealing step. It should be emphasized that these annealing treatments were carried out sequentially on the same proton-implanted CeO_2/Sb_2O_3-co-doped phosphate glass.

Table 1. Conditions of the thermal treatments.

Procedure	Temperature	Time
P_0	As implanted	As implanted
P_1	260 °C	60 min
P_2	310 °C	60 min
P_3	360 °C	60 min

The prism coupling technique can realize optical energy transfer based on the total reflection and evanescent wave. When light propagates inside a prism and enters into the interface between the prism and the waveguide at an angle larger than the critical angle, total reflection occurs. Although light is completely reflected within a prism, an evanescent wave propagating along the interface is excited near the interface. The electromagnetic field distribution of the evanescent wave can extend to the waveguide region and overlap with the guided modes in the waveguide, thereby achieving efficient coupling of optical energy from the prism to the waveguide through phase matching conditions. Therefore, a sharp dip appears on the spectrum. It intuitively indicates that some of the optical field energy has successfully entered into the waveguide through the coupling method, exciting a guided mode. The characteristic parameters, such as amplitude, width, and position of the dip, can be used to evaluate the coupling efficiency, mode selectivity, and waveguide-related characteristics of the optical waveguide, providing an important basis for the subsequent design and optimization of photonic devices.

The end-face coupling technique can record the mode image of the waveguide. During the experiment, the light from the laser is focused onto the end-face of the waveguide through a microscope objective. At the other end of the waveguide, the output beam is collected by an objective lens of the same magnification placed in reverse and directed to the CCD device. The RayCi64 Lite beam analysis software on the computer connected to the CCD is used to obtain the near-field intensity distribution, in order to study the guiding characteristics of the waveguide.

3. Results and discussion

Refractive index is an important parameter in optics and electromagnetics. In general, the refractive index of a substance varies with the wavelength of the measured light source. The refractive index of the CeO_2/Sb_2O_3-co-doped phosphate glass was measured via the prism-coupling system with the resolution of 2×10^{-4}, as illustrated in Fig. 2. It is 1.5294 at 632.8 nm and 1.5151 at 1539 nm, respectively.

Figure 3 is the energy loss distribution based on the SRIM 2013[23] for the H^+ ions with the energy of the 400 keV im-

planted into the CeO_2/Sb_2O_3-co-doped phosphate glass. Towards the end of the range (3.1 μm–4.2 μm), the decelerated ions collide with the target atomic nuclei, ultimately losing a significant amount of the energy and stopping at the end of the range. The accumulation leads to volumetric expansion and reduced density, altering the properties of the original material, and hence resulting in the formation of an optical barrier with a lower refractive index than the substrate material at the accumulation site. Therefore, the hydrogen ion-implanted glass waveguide layer is formed between the air layer and the optical barrier layer.

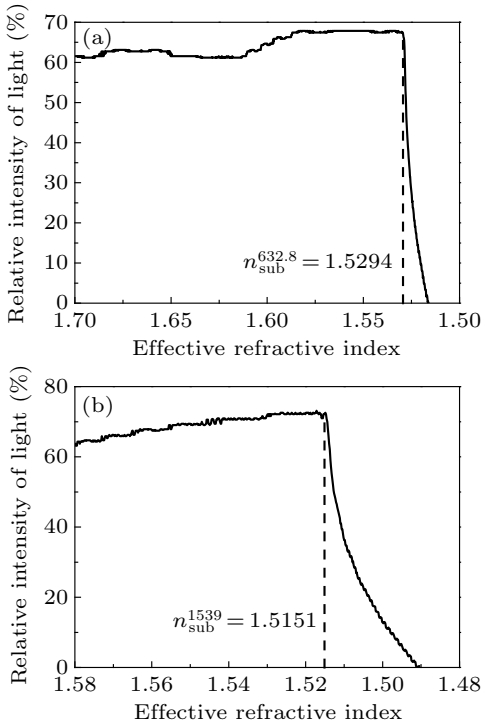


Fig. 2. Refractive index of the CeO_2/Sb_2O_3-co-doped phosphate glass at (a) 632.8 nm and (b) 1539 nm.

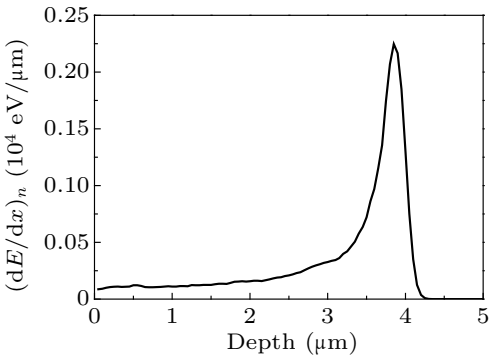


Fig. 3. Energy loss *versus* the depth for the proton implantation into the CeO_2/Sb_2O_3-co-doped phosphate glass.

In Fig. 4, the morphology of the proton-implanted CeO_2/Sb_2O_3-co-doped phosphate glass was obtained through a Nikon microscope. During the observation procedure, the waveguide was vertically placed on a glass slide, where one small end-face of the waveguide is in contact with the glass slide. The light emitted by the source system is transmitted from the bottom to the top of the sample. The microscope objective collects the morphology of the top of the sample. As shown in Fig. 4, there are three layers on the morphology, *i.e.*, air, waveguide core, and substrate. The layer sandwiched between two dashed lines is the waveguide core whose thickness is approximately equal to 3.91 μm.

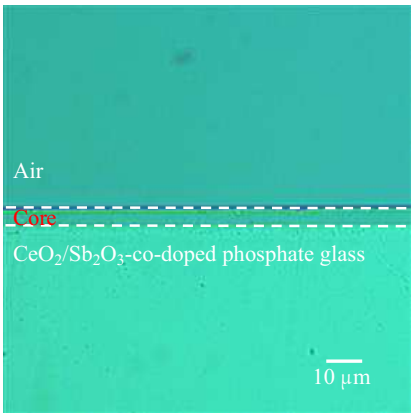


Fig. 4. Cross section of the proton-implanted CeO_2/Sb_2O_3-co-doped phosphate glass.

Figure 5 shows the dark-mode spectra of the as-implanted and annealed ion-implanted CeO_2/Sb_2O_3-co-doped phosphate glass waveguide by the prism-coupling system. There are four dips on the dark-mode spectrum for Figs. 5(a)–5(d). As one can see, for each dark-mode spectrum, the first one is the sharpest and deepest among all four dips. The guided mode corresponding to the dip has good propagation performance in the waveguide. As the number of modes increases, the width of the dip gradually widens. It indicates that the optical constraint of the waveguide on higher-order modes becomes worse.

The dark-mode spectra in Figs. 5(a) and 5(b) are similar in shape, which suggests that the 260-°C annealing treatment has little effect on the waveguide. Compared with Fig. 5(b), the dips on the dark-mode in Fig. 5(c) become more concentrated. This indicates that the performance of the waveguide has been optimized after annealing at 310 °C. However, the dips on the dark-mode in Fig. 5(d) become broad and shallow. This indicates that the ability of the waveguide to confine light has degraded after the 360-°C thermal treatment.

The near-field intensity distribution of the waveguide at 632.8 nm was measured by using an end-face coupling system. Although continuous debugging has been carried out, no light guiding phenomenon has been detected in the proton-implanted CeO_2/Sb_2O_3-co-doped phosphate glass waveguide before the 310-°C annealing and after the 360-°C annealing. Fortunately, the 310-°C annealed waveguide has a limiting effect on the fundamental mode, as displayed in Fig. 6. There are some discontinuities and light leakage on the mode image, which are due to the poor polishing. However, the electromagnetic field of the guided mode can form a stable distribution in

the waveguide. Moreover, the energy of the electromagnetic field for the mode is mainly concentrated in the waveguide core region. The near-field intensity distribution of the waveguide exhibits a bright strip, indicating that the planar structure has the ability to restrict the light propagation. The 632.8-nm signal light propagates in the fundamental mode in the waveguide and is constrained in the vertical direction. Furthermore, based on the system,[24] the propagation loss of the 310-°C annealed waveguide is about 3.2 dB/cm, where the input and output powers are 5.2 mW and 2.5 mW, and the length of the waveguide is 1.0 cm. The 310-°C annealing treatment not only restores partial damage but also reduces propagation loss. Due to the high temperature, the performance of the waveguide has deteriorated for the 360-°C thermal treatment. Therefore, the 310-°C annealed waveguide is demonstrated to be a potential for photonics devices in space exploring and communications.

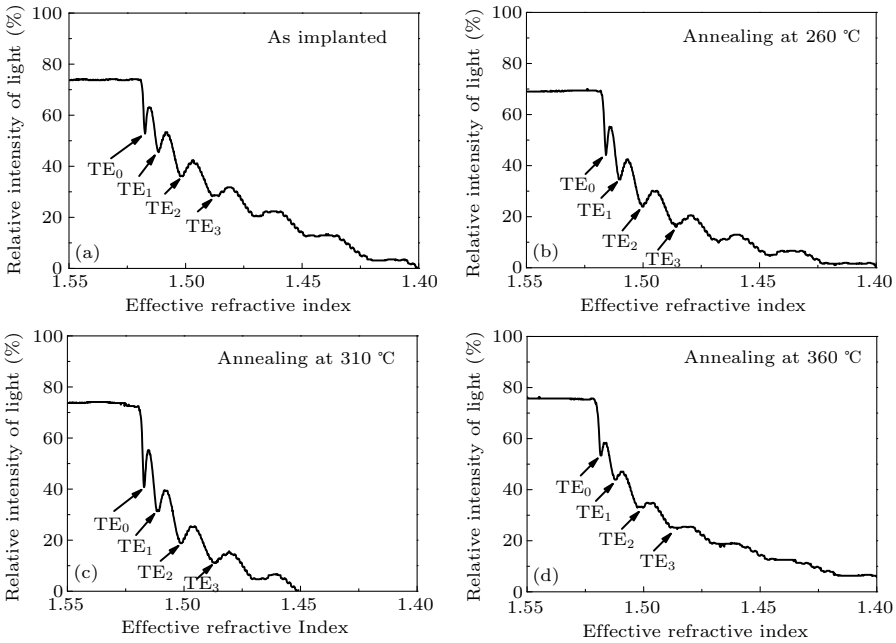


Fig. 5. The *m*-line curves of (a) as-implanted, (b) 260-°C annealed, (c) 310-°C annealed, and (d) 360-°C annealed CeO_2/Sb_2O_3-co-doped phosphate glass waveguides.

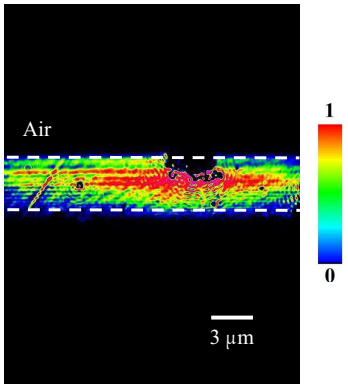


Fig. 6. Near-field mode pattern for the CeO_2/Sb_2O_3-co-doped phosphate glass waveguide after annealing at 310 °C.

The refractive index distribution of the waveguide is reconstructed by using the RCM[25] at 632.8 nm, as Fig. 7 shows. For accuracy and reliability, the first three modes on the dark-mode spectra in Fig. 5 were selected for the reconstruction. Due to the unsatisfactory dark-mode spectrum and the inability to directly guide light, the refractive index distribution of the 360-°C annealed waveguide is not provided here. As one can see, the refractive index distributions of the waveguides are all a typical "optical barrier" type in Figs. 7(a)–7(c). The refractive indices of the core layers for the as-implanted, 260-°C annealed and 310-°C annealed CeO_2/Sb_2O_3-co-doped phosphate glass waveguides were decreased by 0.01, 0.0115, and 0.01, respectively. The annealing at 260 °C is not sufficient to restore the damage and defects caused by the ion implantation, but instead leads to their diffusion. Therefore, the refractive index of the core layer of the 260-°C annealed waveguide is slightly lower than that of the as-implanted waveguide. The 310-°C thermal treatment results in some recovery of damage and defects. The refractive index of the core has been increased to a certain extent. However, in each case the center depth of the optical barrier and the maximum decrease in refractive index at that location are almost both 3.81 μm and 0.0352, respectively.

Table 2 presents the differences between the effective refractive indices of the dark modes measured by the prism coupling experiment and those calculated by the RCM. The calculated values were derived through the continuous adjustment of the refractive index parameters using a least squares program, ensuring that the differences between the experimental and theoretical data fell within an acceptable range. The results in Table 2 show that the relative differences are controlled within the order of 10^{-3}. It suggests that the refractive index distributions of the ion-implanted waveguide in each case are relatively accurate and can reasonably reflect the differences in refractive index across different regions of the waveguide.

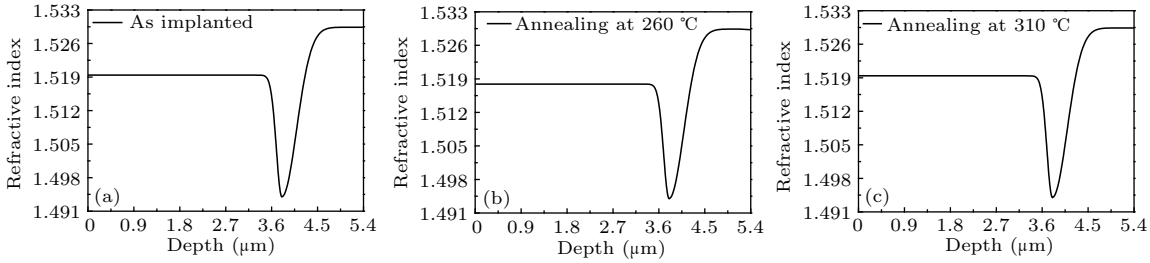


Fig. 7. Refractive index profiles of the (a) as-implanted, (b) 260-°C annealed, and (c) 310-°C annealed CeO_2/Sb_2O_3-co-doped phosphate glass waveguides.

Table 2. Comparisons of experimental and simulated effective refractive indices of the first three modes for the as-implanted and annealed sample.

Procedure	Mode order	Effective refractive index		
		Measurement	Simulation	Difference
P_0	0	1.5174	1.5174	0
	1	1.5115	1.5117	-2.0×10^{-4}
	2	1.5016	1.5020	-4.0×10^{-4}
P_1	0	1.5159	1.5160	-1.0×10^{-4}
	1	1.5104	1.5102	2.0×10^{-4}
	2	1.5001	1.5006	-5.0×10^{-4}
P_2	0	1.5172	1.5174	-2.0×10^{-4}
	1	1.5113	1.5117	-4.0×10^{-4}
	2	1.5012	1.5020	-8.0×10^{-4}

4. Conclusion

The waveguide structure on the CeO_2/Sb_2O_3-co-doped phosphate glass was prepared by proton implantation with an energy of 400 keV and a dose of 8×10^{16} ions/cm^2. A series of annealing treatments were carried out on the waveguide to improve the quality. Under this condition, the peak of the nuclear energy loss is located at a distance of about 3.95 μm from the material surface, which is close to the thickness of the waveguide layer observed by the Nikon microscope. The dark-mode curves of the planar waveguide were obtained and compared using a prism coupler before and after annealing. It was found that the waveguides can operate fundamental mode propagation and the guiding property fluctuates with the annealing conditions. The refractive index distributions of the as-implanted/annealed waveguide were fitted using the reflection calculation method, proving that the waveguide structure is of the "optical barrier" type. The end-face coupling measurement shows that the waveguide has a light limiting ability after annealing at 310 °C for 1 h. It provides a foundation for the formation and optimization of CeO_2/Sb_2O_3-co-doped phosphate glass waveguide devices.

Acknowledgements

Project supported by the Postgraduate Research and Innovation Program of Jiangsu Province, China (Grant No KYCX25_1134), the National Natural Science Foundation of China (Grant No. 11405041), the Key Research and Development Program of Jiangxi Province, China (Grant No. 20223BBE51020), and the Opening Fund of Key Laboratory of Rare Earths (Chinese Academy of Sciences).

References

[1] Xu H, Li Z Q, Pang C, Li R, Li G. L, Akhmadaliev S, Zhou S. Q, Lu Q M, Jia Y C and Chen F 2022 *Chin. Phys. B* **31** 094209
[2] Chen Y H, Jiang Z and He G Q 2023 *Chin. Phys. B* **32** 090306
[3] He S, Yang Q. X, Zhang B, Ren Y Y, Liu H L, Wu P F, Yao Y C and Chen F 2020 *Results Phys.* **18** 103307
[4] Zhang J Y, Chen Y Z, Yang Y C, Wang L L and Liu C X 2024 *Microw. Opt. Techn. Lett.* **66** e34212
[5] Tervonen A, West B R and Honkanen S 2011 *Opt. Eng.* **50** 071107
[6] You J L, Huang X, Lin S Q, Zhang L L, Fu L L, Yue Q Y, Lin S B and Liu C X 2021 *Appl. Opt.* **60** 9146
[7] White A D, Ahn G H, Gasse K V, Yang K Y, Chang L, Bowers J E and Vučković J 2023 *Nat. Photon.* **17** 143
[8] Liu C X, Wang Z H, Guo B E, Yuan R, Wang Y F, Zhou Y H, Sun J B and Zhang L L 2025 *Chin. Phys. B* **34** 054207
[9] Lapointe J, Coia C, Dupont A and Vallée R 2025 *Nat. Photon.* **19** 248
[10] Liu C X, Xing S D, Wang Z H, Li K Y, Sun W and Zhou Y C 2025 *J. Opt. Soc. Am. B* **42** 573
[11] Svecova B, Spirkova J, Janakova S, Mika M, Oswald J and Mackova A 2009 *J. Mater. Sci.: Mater. Electron.* **20** S510
[12] Bai M. Y, Zhao Y. L, Jiao B B, Zhu L J, Zhang G D and Wang L 2018 *Int. J. Mod. Phys. B* **32** 1850170
[13] Jia C L, Li S and Song X X 2017 *Appl. Phys. B* **123** 206
[14] Zhao J H, Li B Y, Bu M Y, Zang W Z, Liu A J, Zhao Y, Yan S, Yue Q Y and Liu Y 2025 *Vacuum* **238** 114218
[15] Wang L L, Cui X J and Liu N Q 2018 *Mod. Phys. Lett. B* **32** 1850288
[16] You J L, Wang Y S, Wang T, Zhang L L, Fu L L, Yue Q Y, Wang X F, Zheng R L and Liu C X 2022 *Chin. Phys. B* **31** 114203
[17] Zhang J N, Zhang T Y, Duan J C, Gong Y X and Zhu S N 2024 *Chin. Phys. B* **33** 110301
[18] He Q L, Wang P F, Sun M Y, Lu M and Peng B 2017 *Opt. Mater. Express* **7** 1113
[19] Kip D 1998 *Appl. Phys. B* **67** 131
[20] Choi D Y, Wade A, Madden S, Wang R P, Bulla D and Luther-Davies B 2013 *Phys. Procedia* **48** 196
[21] Johnson C M, Ridgway M C and Leech P W 1996 *Appl. Phys. Lett.* **69** 984
[22] Wang X L, Wang K M, Fu G, Li S L, Shen D Y, Ma H J and Nie R 2004 *Opt. Express* **12** 4675
[23] Ziegler J F 2023 SRIM-The Stopping and Range of Ions in Matter, http://www.srim.org
[24] Ramponi R, Osellame R and Marangoni M 2002 *Rev. Sci. Instrum.* **73** 1117
[25] Chandler P J and Lama F L 1986 *Opt. Acta* **33** 127